A Journal of the Gesellschaft Deutscher Chemiker

Angewandte International Edition GDCh Chemie

www.angewandte.org

Accepted Article

Title: An Artificial Electrode/Electrolyte Interface for CO2 Electroreduction by Cation Surfactants Self-Assembly

Authors: Yang Zhong, Yan Xu, Jun Ma, Cheng Wang, Siyu Sheng, Congtian Cheng, Mengxuan Li, Lu Han, Linlin Zhou, Zhao Cai, Yun Kuang, Zheng Liang, and Xiaoming Sun

To be cited as: *Angew. Chem. Int. Ed.* 10.1002/anie.202005522

Link to VoR: https://doi.org/10.1002/anie.202005522

WILEY-VCH

10.1002/anie.202005522

WILEY-VCH

RESEARCH ARTICLE

An Artificial Electrode/Electrolyte Interface for CO_2 Electroreduction by Cation Surfactants Self-Assembly

Yang Zhong, Yan Xu, Jun Ma, Cheng Wang, Siyu Sheng, Congtian Cheng, Mengxuan Li, Lu Han, Linlin Zhou, Zhao Cai, Yun Kuang,* Zheng Liang,* Xiaoming Sun*

[*] Y. Zhong, J. Ma, S. Sheng, C. Cheng, M. Li, L. Han, L. Zhou, Prof. Y. Kuang, Prof. X. Sun
State Key Laboratory of Chemical Resource Engineering, Beijing Advanced Innovation Center for Soft Matter Science and Engineering, Beijing University of Chemical Technology Beijing 100029 (China)
E-mail: kuangyun@mail.buct.edu.cn, sunxm@mail.buct.edu.cn
Dr. Y. Xu
Electrical Engineering and Automation, Shandong University of Science and Technology, Tsingtao, 266590, China
Dr. C. Wang
Institute of Water Environmental Research, Chinese Research Academy of Environmental Sciences, Beijing 100012, China
Dr. Z. Cai
Wuhan National Laboratory for Optoelectronics, Huazhong University of Science and Technology, Wuhan 430074, China
Dr. Z. Liang
E-mail: lianzhen@lbl.gov
Materials Sciences Division, Lawrence Berkeley National Laboratory, Berkeley, CA, 94720, USA

Supporting information for this article is given via a link at the end of the document.

Abstract: The electrode/electrolyte (E/E) interface influences the electrocatalytic CO_2 reduction (CO_2RR) behavior by controlling both the diffusion kinetics of the reactants (CO_2/H^+) & products, and the transporting dynamics of the electrons and intermediates. Simultaneous manipulation of the CO_2/H^+ transportation and the interfacial charge transfer would facilitate the CO_2RR process. In this work, we successfully developed an artificial E/E interface construction strategy via coating the electrode surface with quaternary ammonium cation surfactant. This artificial E/E interface with high CO_2 permeability, leads to promoted CO_2 transportation and hydrogenation, as well as suppressed hydrogen evolution (HER). Further study revealed that linear and branched surfactants facilitated formic acid and CO production, respectively. Molecular Dynamics simulations indicated that the artificial interface provided a facile CO_2 diffusion pathway. Moreover, density functional theory (DFT) calculations revealed the stabilization of the key intermediate OCHO* via interacting with the R_4N^+ cations. This surfactant-based artificial interface construction strategy might also be applicable to other electrocatalytic reactions where gas consumption is involved.

Introduction

Electrode/electrolyte (E/E) interface is fundamentally intriguing and essential due to its complex physical and chemical properties. The unique local electric fields, different alkalinity, fast charge and mass transfer all influence the electrochemical processes.[1] Modification of E/E interface could enhance the electrochemical catalytic activity via optimized interfacial electron transfer dynamics and optimized adsorption energy of the reaction intermediates. For gas involving reactions, modification of the E/E interface via superwetting configuration has been proved as an appealing route to drastically alter the transportation efficiency of gas molecules and electrons.[2]

As a prototypical gas consumption reaction, CO_2 electroreduction involves multiple electron and proton transportation, as well as multiple gas diffusion steps.[3] A good electrode for CO_2RR should have active catalytic centers that facilitate the activation of CO_2 molecules and enable unobstructed CO_2 diffusion pathway that favors efficient caption of CO_2. Tremendous efforts have been devoted to the catalysts design, where copper-based nanostructures have been studied extensively due to the capability to produce both one-carbon products (C_1) and multi-carbon products (C_{2+}). Strategies including particles size tuning,[4] facet control,[5] bimetallic and multi-metallic alloying,[6] and metal/metal compound hybrids construction[7] were employed to enhance the intrinsic catalytic activities. These strategies give deep insights into the interactions between catalysts and key intermediates. However, the poor solubility of CO_2 in water (~34 mM at ambient conditions) leads to rapid consumption of CO_2 in the vicinity of the electrode surface, resulting in altered local CO_2/H^+ supply and favored HER.[8]

According to classical catalytic theory, the property of the E/E interface plays the key role in addition to the catalyst itself, which controls the solid/liquid/gas contact, which dominates the kinetics of gas-involved electrocatalytic reactions such as CO_2RR.[9] Electron and mass transfer at this interface are crucial to the electrochemical CO_2 reduction process. Previous report revealed that larger alkali cations could alter the local electric properties of electrode surface thus tuning the selectivity for CO, C_2H_4, and C_2H_5OH,[10] while small organic molecule coating on the electrode surface could alter the adsorption and diffusion behaviors of CO_2.[11] Inspired by these previous reports, herein, we developed an artificial E/E interface enabled by quaternary ammonium cation surfactants (Figure 1). In our study, a Cu-nanowire (Cu NW) electrocatalyst was used as an example to demonstrate this interface design since it has multiple reaction routes and reduction products for CO_2RR with selectivity towards various C_1 and C_{2+} products, as well as the competing hydrogen evolution. With surfactants coating, the selectivity is enhanced compared to

10.1002/anie.202005522

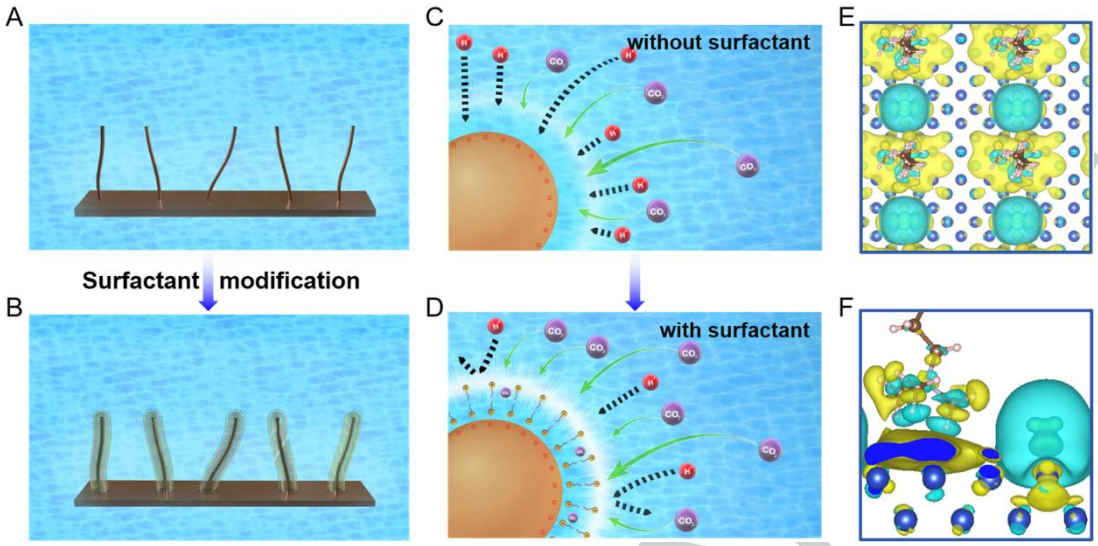

Figure 1. Schematic of quaternary ammonium cation surfactant modification on a Cu nanowire array electrode surface. (A) Schematic of a Cu NW array. (B) Schematic of the Cu NW array after surfactant modification. (C-D) Schematics showing the transportation behaviors of the CO_2 (purple), and H^+ (red) from bulk electrolyte to electrode surface: (C) on pristine Cu NW and (D) on surfactant modified Cu NW. (E-F) The differential charge diagram of a CTAC modified Cu NW surface: (E) top and (F) side view. Yellow region represents the electron accumulation area, blue region represents the electron loss area.

pristine Cu nanowires: Faradaic efficiency of formic acid is increased from 17.8% to 41.8% under CTAC modification, while Faradaic efficiency of CO greatly enhanced from 24.5% to 45.8% with Benzyltriethylammonium chloride (BTEAC) modification. We also find that the Faradaic efficiency of HER is suppressed to below 20%.

Results and Discussion

The cation surfactants were coated on the electrode surface by a drop-casting method (Figure 1A, 1B). The surfactant molecules would assemble into a bilayer structure during the drying process.[12] This cation surfactant interface plays multiple roles in the CO_2RR process: (1) CO_2 molecules have easy access to the catalysts surface through the bilayer region (Figure 1D), especially in use of long chain surfactant molecules. This is because the long hydrocarbon chains provide multiple aerophilic tunnels for CO_2 transportation. Therefore, during continuous bubbling in a H-type cell, the surfactant coated electrode should be able to capture more CO_2 bubbles (detailed discussion in Figure. 3). In contrast to unmodified electrode, as the solubility of CO_2 was quite low, direct contact between the electrode and the electrolyte results in slow CO_2 transportation (Figure 1C). (2) CO_2RR intermediate is able to be stabilized by interacting with $-N^+$ of the adsorbed linear quaternary ammonium cations via charge redistribution. Taking CTAC coating as an example, presence of the surfactant molecules results in negatively-charged surface of the Cu NM electrode (Figure 1E, 1F), thus leading to varied adsorption energy between the electrode and the OCHO* intermediate, a key intermediate towards formic acid production. (3) The surfactant-modified interface weakened the accessibility of protons to the catalyst surface due to electrostatic repulsion between cation surfactants and protons Figure 1D), leading to suppressed HER. In sharp comparison, without surfactant modification, the direct contact between the electrode and the electrolyte unavoidably results in fast proton adsorption due to the hydrophilic nature of metal catalyst, which causes severe HER (Figure 1C).

Among numerous electrocatalysts for CO_2RR, Cu-based materials could produce C_1, C_{2+} products and hydrogen, enabling the study of selectivity towards various products. Cu NWs electrode was chosen as a model electrocatalyst because of its high surface area and uniform structure that are beneficial to a uniform Cu/surfactant interface. The Cu NW was synthesized via chemical etching process followed by annealing and electrochemical reduction. The scanning electron microscopy (SEM, Figure 2A) images show that the surface of Cu foil was uniformly coated with $Cu(OH)_2$ nanowire arrays after chemical etching. The NWs were 100 nm in diameter and tens of micrometers in length (Figure S1A). When annealed in air, these NWs were transformed into CuO with rough surface morphology (Figure S1B). XRD patterns before and after annealing confirmed the phase transformation (Figure S2). Metallic Cu array composed of nanocrystalline grains was obtained via subsequent electrochemical reduction, as evidenced by X-ray photoelectron spectroscopy (XPS) study of the electrode surface (Figure S3). Transmission electron microscope (TEM, Figure 2B) confirmed the rough surface of the Cu NWs, which was composed of nanosized crystalline grains. The lattice fringes measured from Fig. 2b with interplanar spacings of 0.21 nm corresponded to (111) planes of metallic Cu, with numerous grain boundaries observed.

The Cu NW electrode was then modified by quaternary ammonium cation surfactants through a drop-casting method as described above, and the effectiveness of this modification was confirmed by the XPS patterns. Using cetyltrimethylammonium

10.1002/anie.202005522

WILEY-VCH

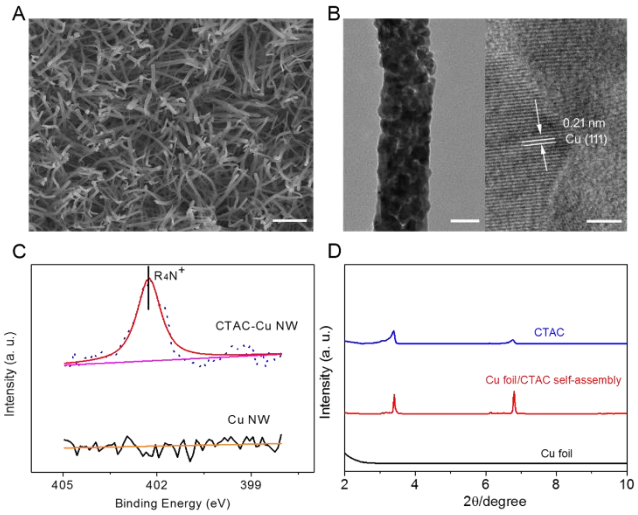

Figure 2. Structural characterization of a CTAC surfactant modified Cu NW array electrode. (A) FESEM of the Cu NW array (Scale bar: 2 um). (B) TEM Image (Scale bar: 50 nm) and HRTEM image of a CTAC surfactant modified Cu NW (Scale bar: 2 nm). (C) N1s scan of the XPS patterns of the Cu NW array electrode before and after CTAC modification. (D) XRD patterns of Cu foil, Cu foil/CTAC self-assembly, and CTAC powders.

chloride (CTAC) as a typical example for the cation surfactant (Figure 2C), a peak at around 400 eV in the N1s spectrum is attributed to the -N^+ group of CTAC, while no signal of nitrogen species was observed for pristine Cu NW. In addition, this peak still existed on the modified Cu NW after CO_2RR (Figure S4), and no NMR signal corresponding to -CH_3 group was detected in the electrolyte when chronoamperomtery test was carried out in N_2-saturated 0.1 M $KHCO_3$ electrolyte for one hour at -0.8 V vs. RHE. This indicated that the CTAC was stable on the Cu NW electrode surface during the electrocatalysis process (Figure S5). In addition, the results combined with N1s XPS spectrum (Figure S4) indicated that the CTAC is not being consumed during CO_2RR process, and all carbonaceous products originate from CO_2 reduction. The adsorption of quaternary ammonium cations on the electrode surface was further confirmed by Fourier transform infrared spectroscopy (FT-IR). Two typical peaks at about 2920 and 2850 cm^{-1} indexed to the stretching vibration of -CH_3 and -CH_2- bond were observed (Figure S6). Energy-dispersive X-ray spectrum (EDX) further confirmed uniform distribution of CTAC on electrode surface (Figure S7). X-ray diffraction (XRD) was utilized to characterize the assembly structures (Fig 2D). Two diffraction peaks at small angels (3.5 degree and 6.9 degree), corresponding to the bilayer and single layer diffraction pattern. In order to further evidence the two peaks were the diffraction of the assembly, we also took the XRD profile of the CTAC powder, in which CTAC molecules would form smectic layer structure stacked along the c-axis [12b]. Two peaks at the same degrees were observed, suggesting the assembly structure and evidencing the bilayer structure of the CTAC assembly on the copper electrode surface. Differential scanning calorimetry (DSC) and Zetapotential analysis further support the bilayer structure(Figure S8, S9).

Linear sweep voltammetry (LSV) was performed to investigate the influence of CTAC on the electrocatalytic activity of Cu NW catalyst in CO_2-purged electrolyte (0.1 M $KHCO_3$, pH 6.8). It is obvious that the electrode modified with CTAC shows largest current density increase relative to pristine Cu NW at the same current densities (Figure 3A), indicating an improved mass transfer. This current density increase confirmed that surfactant coating provided unobstructed CO_2 diffusion pathways. Electrochemical impedance spectroscopy (EIS) was also performed and showed that the contact resistance of the electrode differed little after modification with CTAC (Figure S10A). At a more negative potential, -0.8 V vs. RHE where CO_2RR could happen, the charge transfer resistance of CTAC-modified electrode was lower than that of pristine Cu NW electrode according to the EIS results (Figure S10B), implying a favoured electron transfer for modified electrode during CO_2RR. This suggested that the interaction between Cu NW electrode and cation surfactant could influence the electronic properties of the E/E interface and surface electronic structure change always results in varied electrocatalytic behaviour.

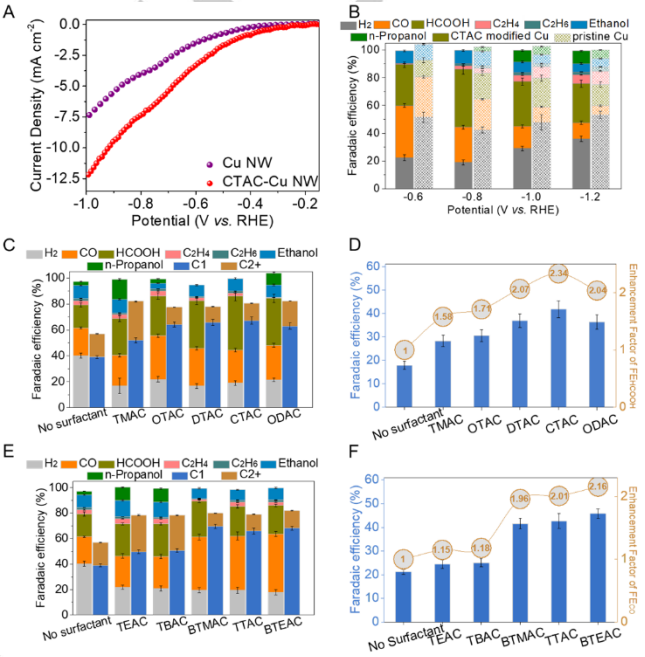

Figure 3. CO_2 electroreduction performances of the Cu NW electrodes with and without surfactant modification. (A) Linear sweep voltammetric curves of the Cu NW electrodes with and without CTAC modification in the CO_2-saturated 0.1 M $KHCO_3$ aqueous solution. With CTAC modification, the overpotential of the electrode showed ~80 mV positive shift at the same current density. (B) Faradaic efficiencies at various potentials of the Cu NW electrodes with and without CTAC. (C) CO_2RR products distributions of the Cu NW electrode modified by different types of liner quaternary ammonium surfactants, data were collected at -0.8 V vs. RHE. (D) FE of formic acid for the Cu electrode modified with different linear surfactants. Data were collected at -0.8 V vs. RHE. Numbers in orange circles show the enhancement factors of FE_{HCOOH}, i.e. FE ratios for formic acid of pristine Cu NW electrodes to modified Cu NW electrode.(E) CO_2RR products distributions of the Cu NW electrodes modified with different types of branched quaternary ammonium surfactants , data were collected at -0.8 V vs. RHE. (F) FE of CO for the Cu NW electrodes modified with different types of branched surfactants. Data were collected at -0.8 V vs. RHE. Numbers in orange circles show the enhancement factors of FE_{CO}, i.e. FE ratios for CO of pristine Cu NW electrode to modified Cu NW electrode.

To unveil the underlying charge transfer mechanism, DFT calculations were performed (Figure S11). For electrodes with linear quaternary ammonium chain length lead to larger negative charged area on the Cu surface, with CTAC modification reaching a maximum value. Specifically, the interaction shows a donation of 0.337 electrons from CTAC to Cu, while 0.250, 0.249, 0.291 for TMAC, OTAC and DTAC, respectively. Additional long chains (ODAC) could not further contribute to electrons donation,

10.1002/anie.202005522

which agreed with the experimental observation that the FE for formic acid was not further enhanced. In addition, the quaternary ammonium cation surfactants modification facilitated the adsorption and activation of CO_2 molecules. In the CO_2RR process, generating $*CO_2^-$ (radical anion) via one electron transfer from the electrode to CO_2 molecule is believed to be the rate-determining step on most catalysts due to the high energy barrier required [13]. Adsorption of OH^- as a surrogate for $*CO_2^-$ to identify the binding affinity to $*CO_2^-$ was carried out under a N_2-bubbled 0.1 M NaOH electrolyte via cyclic voltammetry on the electrode with and without surfactant modification (Figure S12).[13] It was discovered that the peak area for $*CO_2^-$ adsorption on the CTAC modified electrode was higher than that of pristine Cu NW. This suggests that the CTAC modification enhanced CO_2 adsorption to form $*CO_2^-$. The stronger ion pairing resulted in higher intrinsic activity (i.e. 78 mV more positive onset potential of CO_2RR) as compared with pristine Cu NW, which is consistent with the observation from LSV curve (Figure 3A).

To verify the effect of the quaternary ammonium cation surfactants modification on CO_2RR activity and selectivity, the product distributions of Cu NW electrodes with and without surfactants modification were analyzed (Figure 3B). The Faraday efficiencies (FE) of carbonaceous products on pristine Cu NW electrode was quite low due to severe hydrogen evolution reaction in competition (HER). After the quaternary ammonium cation surfactants modification, the HER was suppressed obviously and the FEs of carbonaceous products were enhanced greatly. Setting the reduction potential to -0.8V vs. RHE as a standard condition (the same hereafter if not mentioned), the FE for HER decreased from 40.3% to 19.0% after CTAC surfactant modification, while the total FE for carbonaceous products increased from 56.9% to 80.7% (Figure 3B). Six-hour stability test at -0.8V vs RHE showed that the CTAC-modified Cu NW electrode maintained a stable current density (Figure S13). The adsorbed CTAC surfactant was also very stable on the electrode as could be detected by XPS after 6h stability test (Figure S4). Thus the presence of CTAC could protect the Cu NW from damage (Figure S14C). However, the current density decayed for the pristine Cu NW electrode (Figure S13), along with structural change after 6h CO_2RR (Figure S14D). Such recrystallization due to electrochemical sinter was quite common during CO_2 electroreduction which has often been observed on a hydrophilic Cu surface.[14] It should also be pointed out that the electrochemical active surface area are similar after quaternary ammonium cation surfactants adsorption compared with that of pristine Cu NW (Figure S15), suggesting the selectivity change mainly originated from surfactant modification. In order to further exclude other external influences such as halide anions, which could be adsorbed on the electrode surface and improve CO_2RR selectivity, hexadecyltrimethyl-ammonium hydroxide (CTAH) was used to replace CTAC as a surface modification surfactant. Similar selectivity was found by CTAH modification compared with that of CTAC modification (Figure S16), further evidencing the cation part of the surfactant, CTA^+, played the essential role on selectivity regulation. It is noticeable here that only a small amount of surfactant were used, therefore the influence of surface pH is negligible when considering the diffusion of OH^- from CTAH into bulk electrolyte. In addition, another typical anionic surfactant, sodium dodecyl sulfate (SDS) was used to modify the electrode and its corresponding CO_2RR performance was also tested in 0.1 M $KHCO_3$. However almost no selectivity change was found for SDS-modified Cu NW electrode in comparison to pristine Cu NW electrode (Figure S17). Therefore, it is concluded that quaternary ammonium cations are responsible for the enhanced selectivity for CO_2RR and suppression of HER.

Interestingly, the selectivity for C_1 product, especially the formic acid, varied when electrodes were modified by cation surfactants with different types of hydrocarbon chains. Increasing the linear hydrocarbon chains from 1-C tetramethylammonium chloride (TMAC), to 8-C octyltrimethylammonium chloride (OTAC), 12-C dodecyl trimethyl ammonium chloride (DTAC), and to 16-C cetyltrimethylammonium chloride (CTAC), FE of formic acid gradually increased from 17.8% to 41.8%. An optimal FE_{HCOOH} was achieved under CTAC modification (Figure 3C, 3D, S18). The enhancement factor (the ratio of FE_{HCOOH} of pristine electrodes to that of surfactant-modified electrode) grew from 1.58 tetramethylammonium chloride (TMAC) to 2.34 (CTAC) after long chain surfactants modification (Figure 3D). With the hydrocarbon chain further increasing to 18-C octadecyl dimethyl ammonium chloride (ODAC), the FE_{HCOOH} decreased a little (Figure 3D, S18D), indicating that additional long chains could not contribute to the selectivity regulation. However, further increase of the hydrocarbon chains leads to the decrease of current density due to increased resistance.

Considering the fact that the influence of quaternary ammonium cations on CO_2RR selectivity may be related to the coverage and binding ability to the Cu NW surface (geometric and electronic effects), a series of quaternary ammonium cations with varied branch chain structures, including tetraethylammonium chloride (TEAC), tetrabutylammonium chloride (TBAC), tetraoctylammonium chloride (TTAC), benzyltrimethylammonium chloride (BTMAC) and benzyltriethylammonium chloride (BTEAC) were also investigated. Total C_1 products increased while C_{2+} products decreased when quaternary ammonium surfactants with branched chains were introduced. It was also observed that FE of HER was suppressed from 40.3% to 19.4% after surfactant modification, accompanied by increased FE for total carbonaceous products (Figure 3E). Different from long chain surfactants modification that facilitated formic acid production, modification with branched surfactants increased the selectivity for CO. The enhancement factor (the ratio of FE_{CO} of pristine electrode to that of surfactant-modified electrode) grew from Tetraethylammonium chloride 1.15 (TEAC) to Benzyltriethyl-ammonium chloride 2.16 (BTEAC) after different surfactant modification (Figure 3F, S19). Specifically, when all the branches of quaternary ammonium cations were replaced from methyl to ethyl (TEAC), butyl (TBAC) or octyl (TTAC), the FEs for CO increased from 24.5% to 42.7%, with the trend that the longer the carbon chains of the branches, the higher the FE for CO. Quaternary ammonium surfactants with a benzene ring in the branches (benzyltrimethylammonium chloride, BTMAC) were also employed and it was found that the benzene ring had similar effect to long hydrocarbon branches (FE for CO increased to 41.6% at -0.8 V). Furthermore, when combining both long hydrocarbon branches with benzene ring in the same quaternary ammonium surfactant (Benzyltriethylammonium chloride, BTEAC), the FE for CO was further enhanced (FE for CO increased to 45.8% at -0.8 V).

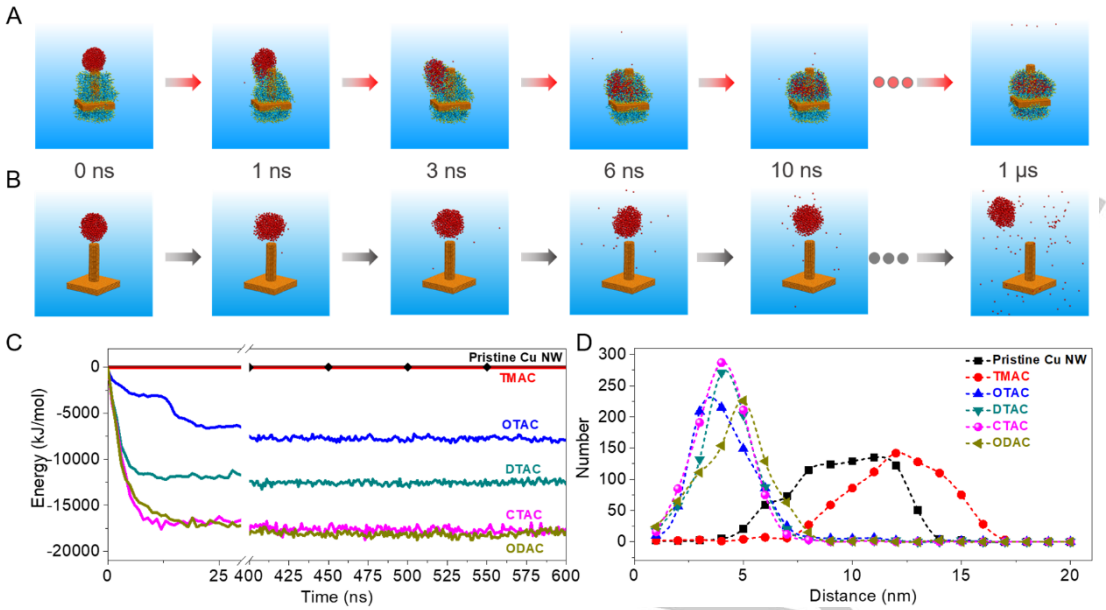

Figure 4. MD simulations of CO_2 diffusion behaviors on the Cu NW surface. Insertion of CO_2 molecules into E/E interface. (A-B) The time sequence of typical snapshots of CO_2 diffusion dynamics on (A) CTAC-modified Cu electrode and (B) pristine Cu electrode. (C) Energy evolution of the system composed of the CO_2 molecules and the Cu electrodes with or without surfactant modification. (D) CO_2 molecule distribution relative to the distance from the electrode surface.

CO_2 reduction usually suffers from slow kinetics due to low local concentration of CO_2 around the electrode, thus competing HER reaction always dominates the electrochemical reduction process. It has been founded in the above section that quaternary ammonium cation surfactants could suppress HER, and that long linear chains of quaternary ammonium cations favor formic acid production while long branched chains prefer CO formation. Based on these two findings, molecular dynamics (MD) simulations and DFT calculations were further utilized to understand the selectivity change. MD simulations provided insights into the molecular-level mechanism of how the CO_2 diffuse into E/E interface from bulk aqueous solution. Time sequence of typical snap-shots of how CO_2 diffuse into E/E interface (Figure 4A and Figure S20) revealed that Cu NW electrode decorated with CTAC was able to capture CO_2 molecules and facilitate CO_2 diffusion, leading to accumulation of CO_2 molecules at E/E interface. However, CO_2 molecules could not easily spread to the Cu NW surface. Instead, most of them stayed at the bulk solution with a slight perturbation (Figure 4B). As for the CTAC-modified electrode surface, the MD simulations revealed that CTAC molecules well covered the Cu NW surface with bilayer assembly structure, which agreed with the XRD (Figure 2D), DSC and Zeta potential characterization (Figure S8-S9). It is worthwhile mentioning that the bilayer CTAC orientation provides an unobstructed CO_2 diffusion pathway ($t < 6$ ns) to minimize the system energy due to hydrophobic (i.e. aerophilic) interaction (Figure 4C).

Similar trend was found on other long chain linear quaternary ammonium surfactants, but not applicable to tetramethylammonium chloride (TMAC). This is because TMAC could not form bilayer structure (Figure S21), and thus it could not provide hydrophobic (i.e. aerophilic) gas transportation pathways. When CO_2 molecules in contact with linear quaternary ammonium cations, the capture of CO_2 from bulk solution is thermodynamically favorable, with a trend that the longer the hydrocarbon chain, the superior CO_2 capture and transportation behavior. CO_2 molecule distribution relative to distance from the electrode surface further confirmed that CO_2 molecules tend to easily accumulate at the electrode surface when quaternary ammonium cations are present (Figure 4D). MD of other linear quaternary ammonium cation surfactants was also investigated (Figures S22-24). CO_2 molecules also tend to accumulate on the modified electrode surface, and CTAC is the optimal choice due to its fastest diffusion for CO_2 and strongest capturing ability of CO_2 molecules on the electrode surface.

In contrary to the liner quaternary ammonium cations that assembled into bilayer structure firmly coating on the Cu electrode surface, branched molecules exhibited different behaviours. Taking tetraoctylammonium chloride (TTAC) as a typical example (Figure S25), TTAC with long branched chains tends to aggregate to form spherical micelles, leading to weak interaction between Cu and the cation surfactant, as evidenced by the NMR signal in the electrolyte after electrolysis (Figure S26). However, CO_2 can still be transported to the electrode surface via diffusion into the micelles, and CO_2RR could still be promoted by collisions of tetraoctylammonium chloride (TTAC) micelle on electrode surface via week electrostatic interaction. MD simulations of other branched quaternary ammonium cations were also investigated (Figure S27, S28) and similar micelle-type CO_2 transportation behaviors were revealed.

Further, the Gibbs free energies for the CO_2RR reaction on the Cu surface with and without surfactant modification were calculated. The Cu (110) surface (Figure S29) was employed to model the experimental systems because it is the exposed facet of the Cu NW. In order to simplify the calculations, TMAC with the shortest hydrocarbon chain was used to model the surfactant coated surface of Cu (110) facet. Since the surfactant was surrounded by a large number of aqueous species, the VASPsol approach was adopted to correct the solvation effect. As shown in Figure S30A, the formation of OCHO* species, a typical intermediate for formic acid formation,[15] is energetically favorable after TMAC modification. Specifically, the ΔG for the

10.1002/anie.202005522

OCHO* species formation is -0.32 eV at Cu/tetramethylammonium chloride (TMAC) interfaces, lower than that of 0.38 eV for the COOH* intermediate. Therefore, surfactant modified Cu surface would stabilize OCHO* and enhance the selectivity for formic acid. However, the COOH* species, a key intermediate for CO pathway, is energetically more favorable at bare Cu surface (Figure S30B), thus the CO production was promoted when branched surfactants were used. This is because branched surfactants could not be adsorbed on the Cu surface (MD simulations results) but could increase the solubility of CO_2.

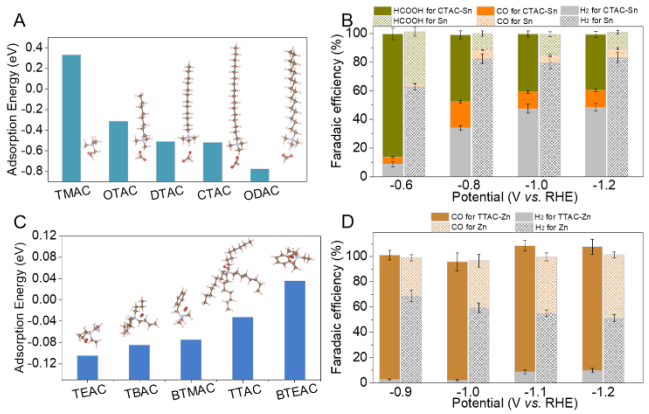

Figure 5. CO_2 electroreduction performances of Sn and Zn electrodes with surfactant modification. (A) The calculated adsorption energy between *OCHO intermediate and various liner quaternary ammonium surfactants. (B) FEs of formic acid at various potentials between Sn foil electrodes with and without CTAC modification (80 μL of 1 mM CTAC modification), data were collected in CO_2-saturated 0.1 M $KHCO_3$ aqueous solution. (C) The calculated adsorption energy between *CO intermediate and various branched quaternary ammonium surfactants. (D) FEs of CO at various potentials between Zn foil electrodes with and without TTAC modification (80 μL of 10 mM TTAC modification), data were collected in CO_2 saturated 0.5 M $KHCO_3$ aqueous solution.

To obtain a deeper understanding of the activity and selectivity enhancement, density functional theory (DFT) calculations were performed to evaluate the strength between the quaternary ammonium cations and the OCHO* specie,[16] which is the intermediate of the CO_2 conversion to formic acid on copper. Figure 5A represents calculated OCHO* adsorption energy against different types of linear molecules. Previous work showed that CO_2RR to formic acid was proceeded via an initial proton-coupled electron transfer to form an intermediate of OCHO*. Here, via plotting the partial current density for formic acid versus *OCHO binding energy, a volcano relationship emerges (Figure S31). According to the classical Sabatier principle, a neither too strong nor too weak binding energy for OCHO* intermediate is essential to improve catalytic performance. It was found that the binding energy for OCHO* on CTAC modified E/E interface had the most suitable value, which accounted for the best activity and selectivity for CO_2RR to formic acid. On the basis of above results, Sn foil, a typical formic acid favored electrocatalyst, was chosen to confirm the enhancing effect. It was observed that the FEs for formic acid increased from 36.3% to 85.9% at -0.6 V after CTAC modification (Figure 5B). Similar enhancements were found on all other testing potentials, suggesting CTAC modification was a general way to facilitate CO_2RR for formic acid production.

Similarly, DFT calculations were performed to evaluate the strength between the branch quaternary ammonium cations and the CO* species, which is the intermediate for CO production. It was found that increasing the chain length of the branches or introducing benzene ring into the branch decreased the affinity to *CO species. The combination of long chain branches and benzene ring in BTEAC maximized this trend and this surfactant could even repel the *CO species, thus favors CO desorption, which is the rate-limiting step for CO production (Figure 5C). Therefore, the weaker the interaction between the branch quaternary ammonium cations and the CO* species, the higher the selectivity for CO production. In order to investigate the universality of branched surfactant modification, we applied TTAC modification on Zn foil, an electrocatalyst that favors CO production intrinsically. Impressively, the FE for CO increased from ~30% to above 90% over all the testing potentials (Figure 5D). From the results we have obtained, it can be concluded that this interface modification strategy by cation surfactants provides a new route in the development of advanced electrode for electrocatalysis besides catalyst design.

Conclusion

In summary, surfactants modification was an efficient strategy to construct an artificial interface for activity and selectivity regulation of CO_2 electroreduction. Introduction of quaternary ammonium cation surfactants favors CO_2 transportation while limits proton supply to the electrode surface, enabling enhanced total FE for carbonaceous products. Further study revealed that linear long chains of quaternary ammonium cation surfactants boost formic acid formation while branched long chains of quaternary ammonium cation surfactants favor CO production. Both electronic effects and geometric effects derived from quaternary ammonium cations contribute to the selectivity variation of CO_2RR. The unique E/E interface structure, quaternary ammonium cations on the surface of Cu endow the Cu-surfactant electrodes with high catalytic activities and tunable selectivity. This study provides a new tool and deep insight on how interface regulates charge and mass transfer, and therefore, the strategy may be potentially applicable to other electrocatalytic gas consumption systems, such as oxygen reduction reaction (ORR), hydrogen oxidation reaction (HOR), nitrogen/nitrogen-oxide reduction reaction (N_2RR/NO_xRR) etc.

Acknowledgements

This work was supported by the National Natural Science Foundation of China (NSFC), the National Key Research and Development Project (No. 2018YFB1502401, 2018YFA0702002), the Royal Society and the Newton Fund through the Newton Advanced Fellowship award (NAF\R1\191294), the Program for Changjiang Scholars and Innovation Research Team in the University (No. IRT1205), the Fundamental Research Funds for the Central Universities, and the long-term subsidy mechanism from the Ministry of Finance and the Ministry of Education of PRC.

Keywords: CO_2 reduction • electrode/electrolyte interface • cation surfactant • gas diffusion

[1] a) R. Subbaraman, D. Tripkovic, D. Strmcnik, K. C. Chang, M. Uchimura, A. P. Paulikas, V. Stamenkovic, N. M. Markovic, *Science* **2011**, *334*, 1256-1260; b) V. R. Stamenkovic, D. Strmcnik, P. P. Lopes, N. M. Markovic, *Nat Mater* **2016**, *16*, 57-69; c) A. Bagger, L. Arnarson, M. H. Hansen, E. Spohr, J. Rossmeisl, *J Am Chem Soc* **2019**, *141*, 1506-1514; d) C. T. Dinh, T. Burdyny, M. G. Kibria, et al., *Science* **2018**, *360*, 783-787.

[2] a) W. Xu, Z. Lu, X. Sun, L. Jiang, X. Duan, *Acc Chem Res* **2018**, *51*, 1590-1598; b) Y. Shi, B. Zhang, *Chem Soc Rev* **2016**, *45*, 1529-1541; c) Z. Cai, Y. Zhang, Y. Zhao, Y. Wu, W. Xu, X. Wen, Y. Zhong, Y. Zhang, W. Liu, H. Wang, Y. Kuang, X. Sun, *Nano Research* **2018**, *12*, 345-349; d) J. Li, G. Chen, Y. Zhu, Z. Liang, A. Pei, C.-L. Wu, H. Wang, H. R. Lee, K. Liu, S. Chu, Y. Cui, *Nature Catalysis* **2018**, *1*, 592-600; e) Z. Lu, W. Xu, J. Ma, Y. Li, X. Sun, L. Jiang, *Adv Mater* **2016**, *28*, 7155-7161.

[3] a) M. B. Ross, P. De Luna, Y. Li, C.-T. Dinh, D. Kim, P. Yang, E. H. Sargent, *Nature Catalysis* **2019**, *2*, 648-658; b) Y. Zheng, A. Vasileff, X. Zhou, Y. Jiao, M. Jaroniec, S. Z. Qiao, *J Am Chem Soc* **2019**, *141*, 7646-7659.

[4] R. Reske, H. Mistry, F. Behafarid, B. Roldan Cuenya, P. Strasser, *J Am Chem Soc* **2014**, *136*, 6978-6986.

[5] a) C. Choi, T. Cheng, M. Flores Espinosa, H. Fei, X. Duan, W. A. Goddard, 3rd, Y. Huang, *Adv Mater* **2019**, *31*, e1805405; b) C. Hahn, T. Hatsukade, Y. G. Kim, A. Vailionis, J. H. Baricuatro, D. C. Higgins, S. A. Nitopi, M. P. Soriaga, T. F. Jaramillo, *Proc Natl Acad Sci USA* **2017**, *114*, 5918-5923.

[6] a) S. Lee, G. Park, J. Lee, *ACS Catalysis* **2017**, *7*, 8594-8604; b) E. L. Clark, C. Hahn, T. F. Jaramillo, A. T. Bell, *J Am Chem Soc* **2017**, *139*, 15848-15857; c) S. Ma, M. Sadakiyo, M. Heima, R. Luo, R. T. Haasch, J. I. Gold, M. Yamauchi, P. J. Kenis, *J Am Chem Soc* **2017**, *139*, 47-50; d) A. Vasileff, C. Xu, Y. Jiao, Y. Zheng, S.-Z. Qiao, *Chem* **2018**, *4*, 1809-1831.

[7] P. Wang, M. Qiao, Q. Shao, Y. Pi, X. Zhu, Y. Li, X. Huang, *Nat Commun* **2018**, *9*, 4933.

[8] a) D. M. Weekes, D. A. Salvatore, A. Reyes, A. Huang, C. P. Berlinguette, *Acc Chem Res* **2018**, *51*, 910-918; b) F. Pelayo García de Arquer; C. T. Dinh, A. Ozden, J. Wicks, C.Mccallum, A. R. Kirmani, et al., *Science*, **2020**, 367, 661–666.

[9] Z. W. Seh, J. Kibsgaard, C. F. Dickens, I. Chorkendorff, J. K. Norskov, T. F. Jaramillo, *Science* **2017**, *355*, eaad4998.

[10] a) M. R. Singh, Y. Kwon, Y. Lum, J. W. Ager, 3rd, A. T. Bell, *J Am Chem Soc* **2016**, *138*, 13006-13012; b) S. Ringe, E. L. Clark, J. Resasco, A. Walton, B. Seger, A. T. Bell, K. Chan, *Energy & Environmental Science* **2019**; c) J. Resasco, L. D. Chen, E. Clark, C. Tsai, C. Hahn, T. F. Jaramillo, K. Chan, A. T. Bell, *J Am Chem Soc* **2017**, *139*, 11277-11287.

[11] a) D. Wakerley, S. Lamaison, F. Ozanam, N. Menguy, D. Mercier, P. Marcus, M. Fontecave, V. Mougel, *Nat Mater* **2019**; b) M. S. Xie, B. Y. Xia, Y. Li, Y. Yan, Y. Yang, Q. Sun, S. H. Chan, A. Fisher, X. Wang, *Energy & Environmental Science* **2016**, *9*, 1687-1695; c) F. Li, A. Thevenon, A. Rosas-Hernandez, Z. Wang, Y. Li, C. M. Gabardo, A. Ozden, C. T. Dinh, J. Li, Y. Wang, J. P. Edwards, Y. Xu, C. McCallum, L. Tao, Z. Q. Liang, M. Luo, X. Wang, H. Li, C. P. O'Brien, C. S. Tan, D. H. Nam, R. Quintero-Bermudez, T. T. Zhuang, Y. C. Li, Z. Han, R. D. Britt, D. Sinton, T. Agapie, J. C. Peters, E. H. Sargent, *Nature* **2020**, *577*, 509-513. d) A. K. Buckley, M. Lee, T. Cheng, R. V. Kazantsev, D. M. Larson, W. A. Goddard Iii, F. D. Toste, F. M. Toma, *J Am Chem Soc* **2019**, *141*, 7355-7364. e) S. Banerjee, X. Han, V. S. Thoi, *ACS Catalysis* **2019**, *9*, 5631-5637.

[12] a)T. Inaba, Y. Takenaka, Y. Kawabata, T. Kato, *J Phys Chem B* **2019**, *123*, 4776-4783. b) K. Okuyama, T. Ishii, K. Vongbupnimit, K. Noguchi, *Molecular Crystals and Liquid Crystals Science and Technology. Section A. Molecular Crystals and Liquid Crystals*, **2006**, *312*, 101-115.

[13] a)F. Lei, W. Liu, Y. Sun, J. Xu, K. Liu, L. Liang, T. Yao, B. Pan, S. Wei, Y. Xie, *Nat Commun* **2016**, *7*, 12697. b) H. Xie, T. Wang, J. Liang, Q. Li, S. Sun, *Nano Today* **2018**, *21*, 41-54.

[14] Y. Li, F. Cui, M. B. Ross, D. Kim, Y. Sun, P. Yang, *Nano Lett* **2017**, *17*, 1312-1317.

[15] a) X. Zheng, P. De Luna, F. P. García de Arquer, B. Zhang, N. Becknell, M. B. Ross, Y. Li, M. N. Banis, Y. Li, M. Liu, O. Voznyy, C. T. Dinh, T. Zhuang, P. Stadler, Y. Cui, X. Du, P. Yang, E. H. Sargent, *Joule* **2017**, *1*, 794-805; b) N. Han, Y. Wang, H. Yang, J. Deng, J. Wu, Y. Li, Y. Li, *Nat Commun* **2018**, *9*, 1320.

[16] D. Niu, H. Wang, H. Li, X. Zhang, *Electrochemistry Communications* **2015**, *52*, 58-62.

10.1002/anie.202005522

Entry for the Table of Contents

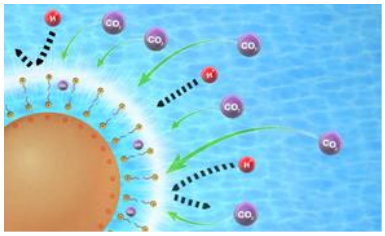

An artificial quaternary ammonium cation surfactant E/E interface construction strategy change the CO_2RR pathway. MD simulations indicated that the artificial interface provided a facile CO_2 diffusion pathway. DFT calculations revealed the stabilization of the key intermediates via interacting with the R_4N^+ cations.

Institute and/or researcher Twitter usernames: ((optional))